Ionic Hydrogenation of Ketones with Molybdenum Pentabenzylcyclopentadienyl Hydride Catalysts†

Sónia Namorado, Maria Augusta Antunes, Luis F. Veiros, José R. Ascenso, M. Teresa Duarte, and Ana M. Martins*

Centro de Química Estrutural, Instituto Superior Técnico, Av. Rovisco Pais, 1049-001 Lisboa, Portugal

Received April 30, 2008

A study of the reactivity of $[MoCp^{Bz}(CO)_3H]$ (Cp^{Bz} = pentabenzylcyclopentadienyl) as a catalyst precursor for the ionic hydrogenation of 3-pentanone is presented. The complexes $[MCp^{Bz}(CO)_3OTf]$ (M = Mo (**3**), W (**4**)), $[MoCp^{Bz}(CO)_3(O{=}CEt_2)]BF_4$ (**9**), and $[MoCp^{Bz}(CO)_3(O{=}CMe_2)]BF_4$ (**12**) are described. $\mathbf{9}^+$ and $[MoCp^{Bz}(CO)_3(OHCHEt_2)]^+$ ($\mathbf{8}^+$) were identified by NMR under catalytic conditions. The reaction of $[WCp^{Bz}(CO)_3H]$ with triflic acid led to $[WCp^{Bz}(CO)_3(H)_2]^+$ ($\mathbf{7}^+$), which was identified by NMR as a dihydride complex. The influence of steric and electronic effects on the catalyst activity is discussed on the basis of experimental results and a mechanism proposal resulting from DFT calculations. The proposed mechanism includes facile protonation of the acetone O atom promoted by a dihydride Mo(IV) complex, followed by slower hydride transfer from the metal center to the carbonyl C atom. The results indicate strong coordination of both the product (isopropyl alcohol) and the reactant (acetone), leading to some blocking of the catalyst active site. Regeneration of the catalyst active species is the rate-limiting step of the catalytic cycle. The steric bulk of the Cp^{Bz} ligand increases the catalyst activity.

Introduction

The reduction of ketones to alcohols by an ionic mechanism is an important reaction that has attracted much interest.[1−7] In the presence of strong acids the oxygen atom of ketones is protonated and the subsequent hydride transfer from a transition-metal hydride complex completes the reduction of the C═O group. Studies on the protonation of $[WCp(CO)_2(PMe_3)H]$ have shown that the extent of the reaction depends on the solvents and the formation of acid/base homoconjugate pairs. Although a nonclassical η^2-H_2 ligand has not been directly observed, the kinetic site of protonation is the hydride ligand.[8] The cationic dihydrides $[WCp(CO)_2(PR_3)(H)_2]^+$ have been observed at low temperatures by NMR[9,10] and by X-ray diffraction (R = Me).[10] The hydricity of complexes $[MCp'(CO)_{3-n}(PR_3)_nH]$ (Cp′ = Cp, Cp*, Ind; R = Me, Ph, Cy; n = 0, 1; M = Cr, Mo, W) shows that (i) phosphine-containing compounds are better hydride sources, (ii) hydride transfer is faster for trans isomers, and (iii) cis/trans isomerization may be the limiting step of hydride transfer reactions.[11,12]

Recently Bullock and co-workers have turned the ionic reduction of ketones into a true hydrogenation catalytic reaction.[13] Using as catalyst precursors $[MoCp(CO)_2(PR_3)H]$ and the trityl cation, the complexes catalyze the reduction of 3-pentanone in the presence of hydrogen. The influence of the phosphine ligands on the catalyst activity revealed a dependence on the phosphine cone angles, and the dissociation of PR_3 was identified as a decomposition pathway of the catalysts.[14,15] Replacement of phosphine by an N-heterocyclic carbene led to inefficient ketone hydrogenation catalysts, due to the vulnerability of carbene ligands to protonation, producing an imidazolium cation.[16]

Our interest in molybdenum and tungsten pentabenzylcyclopentadienyl complexes[17−19] led us to assess the properties of $[MCp^{Bz}(CO)_3H]$ in the catalytic hydrogenation of ketones. The lack of ligands susceptible to participate in the catalyst decomposition and the influence of a very bulky cyclopentadienide ligand in the ionic hydrogenation of ketones catalyzed

* To whom correspondence should be addressed. E-mail: ana.martins@ist.utl.pt.

† This paper is dedicated to the memory of Professor Alberto R. Dias.

(1) Gaus, P. L.; Kao, S. C.; Youngdahl, K.; Darensbourg, M. Y. *J. Am. Chem. Soc.* **1985**, *107*, 2428–2434.
(2) Gibson, D. H.; El-Omrani, Y. S. *Organometallics* **1985**, *4*, 1473–1475.
(3) Geraty, S. M.; Harkin, P.; Vos, J. G. *Inorg. Chim. Acta* **1987**, *131*, 217–220.
(4) Song, J.-S.; Szalda, D. J.; Bullock, R. M.; Lawrie, J. C.; Rodkin, M. A.; Norton, J. R. *Angew. Chem., Int. Ed. Engl.* **1992**, *31*, 1233–1235.
(5) Bakhmutov, V. I.; Vorontsov, E. V.; Antonov, D. Y. *Inorg. Chim. Acta* **1998**, *278*, 122–126.
(6) Reynoud, J. F.; Leboeuf, J. F.; Leblanc, J. C.; Moise, C. *Organometallics* **1986**, *5*, 1863–1866.
(7) Song, J.-S.; Szalda, D.; Bullock, R. M. *Inorg. Chim. Acta* **1997**, *259*, 161–172.
(8) Papish, E. T.; Rix, F. C.; Spetseris, N.; Norton, J. R.; Williams, R. D. *J. Am. Chem. Soc.* **2000**, *122*, 12235–12242.
(9) Ryan, O. B.; Tilset, M.; Parker, V. D. *J. Am. Chem. Soc.* **1990**, *112*, 2618–2626.
(10) Bullock, R. M.; Song, J.-S.; Szalda, D. *Organometallics* **1996**, *15*, 2504–2516.
(11) Smith, K.-T.; Norton, J. R.; Tilset, M. *Organometallics* **1996**, *15*, 4515–4520.
(12) Cheng, T. Y.; Brunschwig, B. S.; Bullock, R. M. *J. Am. Chem. Soc.* **1998**, *120*, 13121–13137.
(13) Bullock, R. M.; Voges, M. H. *J. Am. Chem. Soc.* **2000**, *122*, 12594–12595.
(14) Voges, M. H.; Bullock, R. M. *Dalton Trans.* **2002**, 759–770.
(15) Bullock, R. M. *Chem. Eur. J.* **2004**, *10*, 2366–2374.
(16) Wu, F.; Dioumaev, V. K.; Szalda, D. J.; Hanson, J.; Bullock, R. M. *Organometallics* **2007**, *26*, 5079–5090.
(17) Martins, A. M.; Branquinho, R.; Cui, J. L.; Dias, A. R.; Duarte, M. T.; Fernandes, J.; Rodrigues, S. S. *J. Organomet. Chem.* **2004**, *689*, 2368–2376.
(18) Martins, A. M.; Romão, C. C.; Abrantes, M.; Azevedo, M. C.; Cui, J. L.; Dias, A. R.; Duarte, M. T.; Lemos, M. A.; Lourenco, T.; Poli, R. *Organometallics* **2005**, *24*, 2582–2589.
(19) Namorado, S.; Cui, J. L.; de Azevedo, C. G.; Lemos, M. A.; Duarte, M. T.; Ascenso, J. R.; Dias, A. R.; Martins, A. M. *Eur. J. Inorg. Chem.* **2007**, *110*, 3–1113.

10.1021/om800379z CCC: $40.75
Publication on Web 08/26/2008

Scheme 1

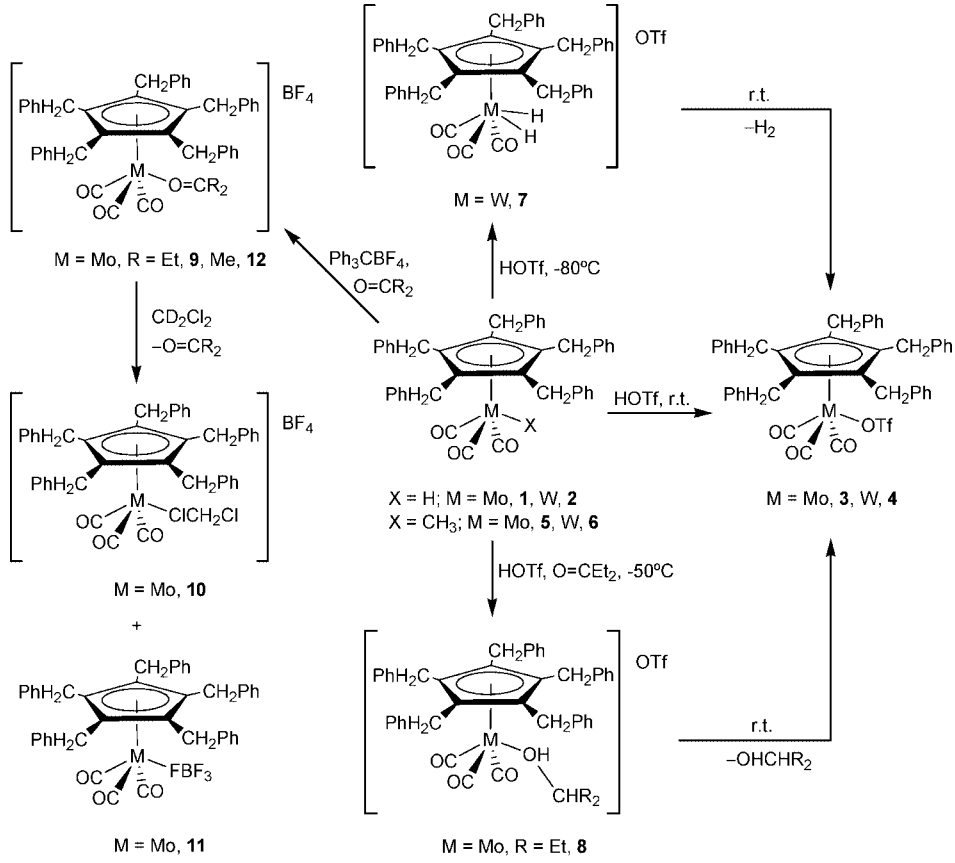

by molybdenum hydrides are discussed and related to a DFT[20] study of the reaction mechanism.

Results and Discussion

Chemical Studies. Syntheses and Characterization. All new compounds are represented in Scheme 1. Addition of dichloromethane solutions of triflic acid to equimolar amounts of the metal hydrides $[MCp^{Bz}(CO)_3H]$ (M = Mo (**1**), W (**2**); Cp^{Bz} = pentabenzylcyclopentadienyl)[19] dissolved in the same solvent resulted in immediate darkening of the light yellow solutions. The reactions led to the formation of the complexes $[MCp^{Bz}(CO)_3OTf]$ (M = Mo (**3**), W (**4**)), which were isolated in high yields as red crystals (M = Mo, 94% yield) and a microcrystalline orange solid (M = W, 92% yield). Complexes **3** and **4** may alternatively be obtained by reactions of $[MCp^{Bz}(CO)_3Me]$ (M = Mo (**5**), W (**6**)) with HOTf in similar yields.

The IR spectra of **3** and **4** show three absorption bands for the carbonyl ligands at values slightly higher than those reported for other $[MCp^{Bz}(CO)_3X]$ complexes[17,21] but shifted to lower values when compared to those reported for $[MCp(CO)_3OTf]$ (M = Mo, W)[22] (Table 1). This shows that metal−carbonyl back-bonding is more extensive in **3** and **4** than in analogous Cp derivatives, and thus, the five benzyl substituents on the Cp ring make the pentabenzylcyclopentadienide ligand a better donor than cyclopentadienide. The IR spectra also display a series of peaks centered at ca. 3000 cm^{-1} and below 1600 cm^{-1} characteristic of the Cp^{Bz} ligand and three bands assigned to the $\nu_{as}(SO_3)$ and $\nu_s(SO_3)$ bands of the coordinated triflate group. The ^1H NMR spectra of complexes **3** and **4** show one singlet corresponding to the methylenic protons (δ (CD_2Cl_2) 3.73 ppm for **3** and 3.80 ppm for **4**) and two multiplets in the aromatic region, indicating that there are no constraints to the free rotation of the five benzyl groups in solution. Accordingly the ^{13}C NMR spectra present one resonance for the methylenic carbons, one resonance for the Cp ring carbons, four benzyl aromatic carbon resonances, and two resonances for the carbonyl carbons that are integrated 2:1, as expected for four-legged piano-stool metal coordination. The ^{19}F NMR spectra exhibit one singlet at δ −77.4 ppm for **3** and δ −76.8 ppm for **4**, assigned to the fluorine atoms of the triflate group.

Table 1. IR Carbonyl Frequencies (cm^{-1})

compd	ν(C≡O)		
3	2058	1981	1956
$[MoCp^{Bz}(CO)_3Cl]$	2041	1975	1956
$[MoCp^{Bz}(CO)_3Me]$	2011	1934	1919
$[MoCp^{Bz}(CO)_3H]$	2008	1928	1822
$[MoCp(CO)_3OTf]$	2073	1995	1962
4	2050	1968	1947
$[WCp^{Bz}(CO)_3Cl]$	2032	1967	1942
$[WCp^{Bz}(CO)_3Me]$	2009	1926	1893
$[WCp^{Bz}(CO)_3H]$	2008	1901	
$[WCp(CO)_3OTf]$	2067	1982	1945

Dark red needles of **3** and orange crystals of **4** suitable for single-crystal X-ray diffraction determination were obtained from diethyl ether solutions at −20 °C. The compound molecular structures depicted in Figures 3 and 4 are discussed later.

Reactions of **1** and **2** with HOTf were carried out in sealed NMR tubes and studied by ^1H and ^{19}F NMR. Upon addition of

(20) Parr, R. G.; Yang, W. *Density Functional Theory of Atoms and Molecules*; Oxford University Press: New York, 1989.

(21) Song, L. C.; Zhang, L. Y.; Hu, Q. M.; Huang, X. Y. *Inorg. Chim. Acta* **1995**, *230*, 127–131.

(22) Appel, M.; Schloter, K.; Heidrich, J.; Beck, W. *J. Organomet. Chem.* **1987**, *322*, 77–88.

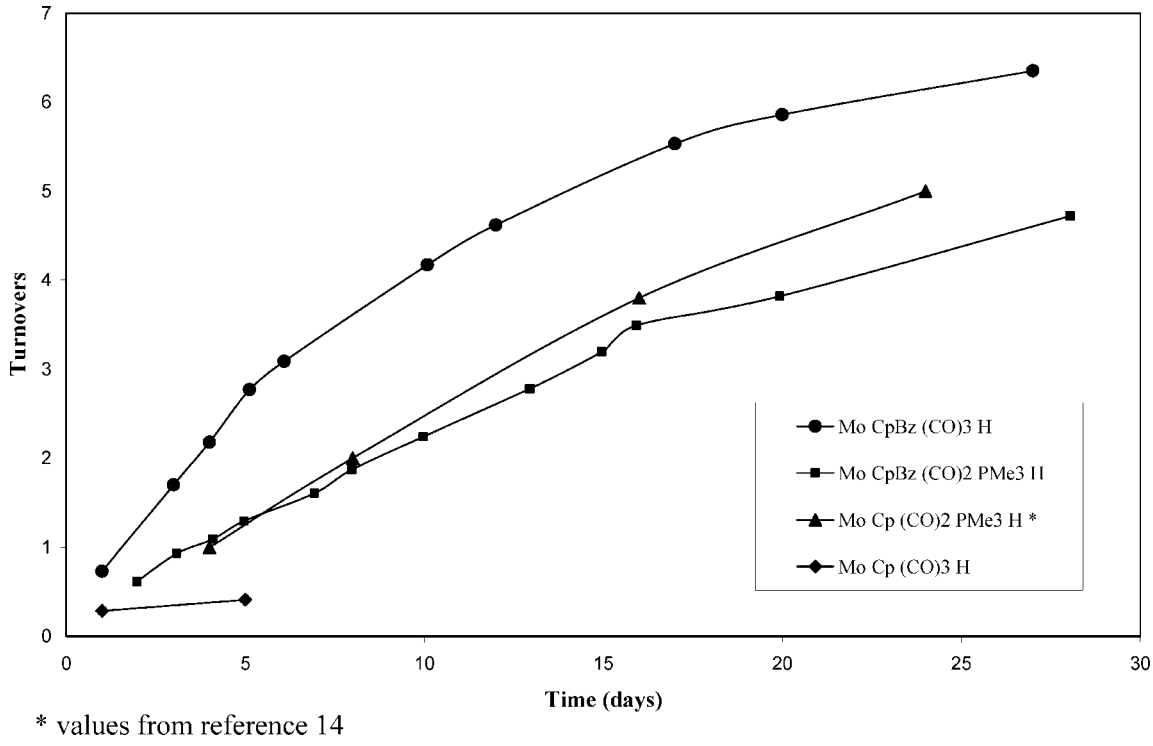

Figure 1. Catalytic hydrogenation of 3-pentanone with $[MoCp'(CO)_{3-n}(PMe_3)_nH]$ ($Cp' = Cp, Cp^{Bz}$, $n = 0, 1$) catalysts in CD_2Cl_2 (catalyst: ketone = 1:10, $P(H_2) = 4$ atm).

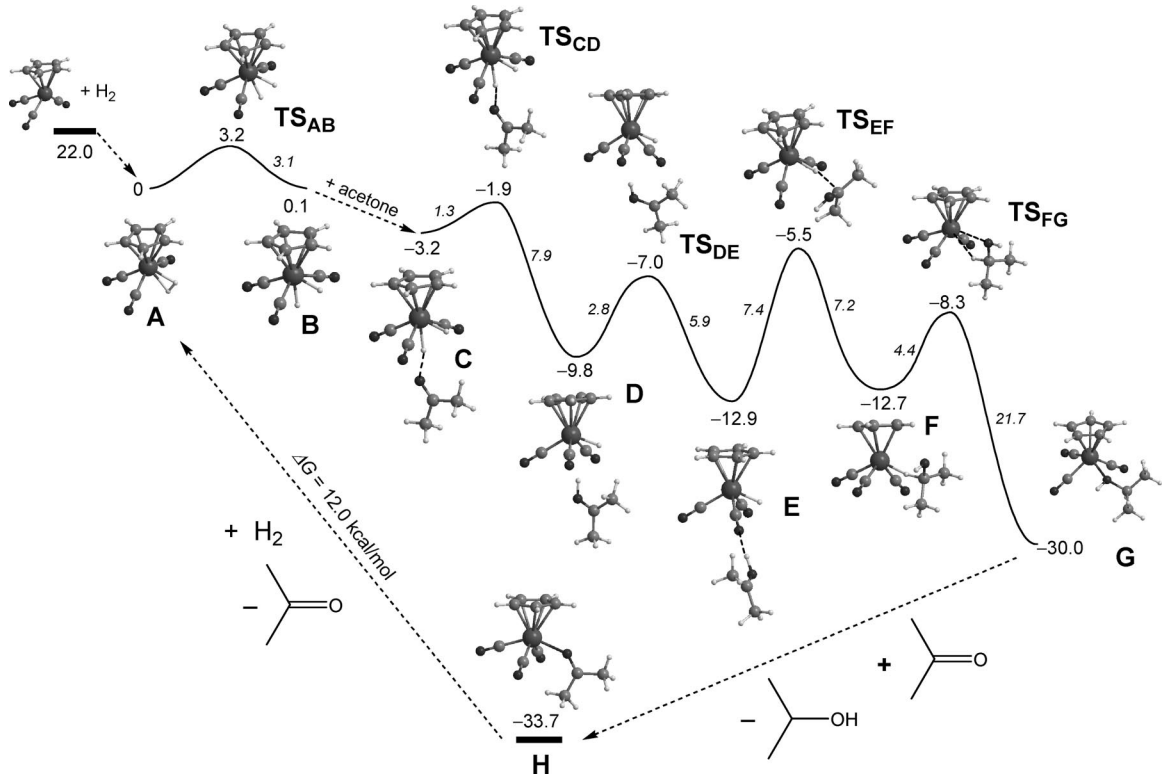

Figure 2. Free energy profile calculated (PBE1PBE) for the hydrogenation of acetone catalyzed by $[MoCp(CO)_3]^+$. The minima and transition states were optimized, and the structures obtained are present. Free energies (kcal/mol) are referred to the dihydrogen complex $[MoCp(CO)_3(H)_2]^+$ (**A**), and the values in italics represent energy barriers.

1 equiv of HOTf to a frozen solution of **2** in CD_2Cl_2, the tube was sealed under vacuum and the temperature of the mixture was raised to −80 °C. The formation of a new species, identified as the dihydride $[WCp^{Bz}(CO)_3(H)_2]OTf$ (**7**), was detected by the appearance of a new resonance at δ −1.96 ppm. The assignment of this resonance was based on the spin−lattice relaxation time (T_1) criterion described by Crabtree, which allows one to distinguish between dihydride and dihydrogen ligands.[23−25] According to this, short T_1 values (4−100 ms) are observed for dihydrogen ligands, whereas classical dihydride

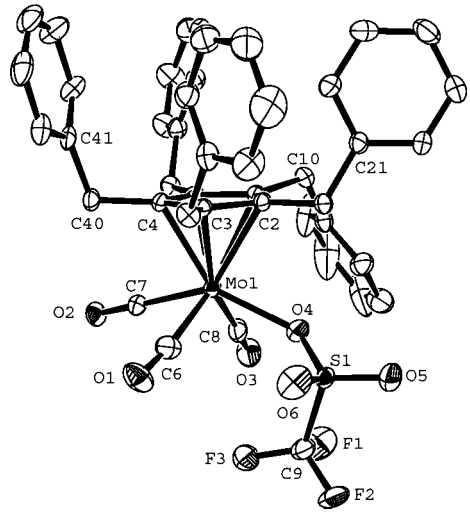

Figure 3. Molecular structure of **3** showing thermal ellipsoids at the 50% probability level. Hydrogen atoms and disordered solvent molecules are omitted for clarity.

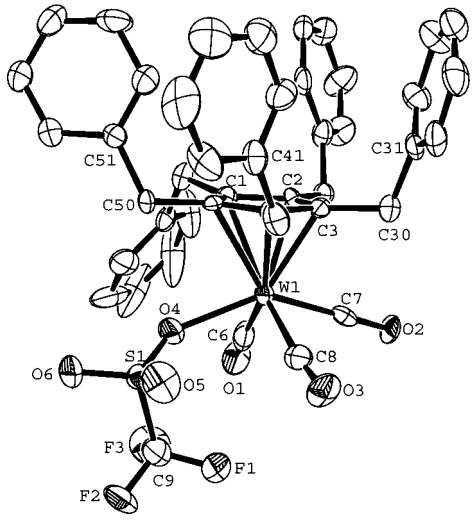

Figure 4. Molecular structure of **4** showing thermal ellipsoids at the 50% probability level. Hydrogen atoms and disordered solvent molecules are omitted for clarity.

species cause significantly longer T_1 values, reflecting longer H···H distances. A value of 472 ms, which is consistent with a dihydride formulation, was determined for **7** at −70 °C, when the T_1 vs temperature curve reaches the minimum. At this temperature the integration of the new signal at −1.96 ppm versus the hydride resonance in **2** (−6.72 ppm) revealed 50% conversion of **2** into **7**. As the temperature was raised, broadening of all hydride resonances was observed. Simultaneously, the two sets of resonances assigned to the benzylic protons of the Cp^{Bz} ligands in **2** and **7** overlapped, and when the temperature reached −10 °C, the hydride resonances of both species collapsed into the baseline. At 10 °C a new resonance due to the methylenic protons of the triflate derivative **4** appeared at δ 3.76 ppm. Cooling the sample to −80 °C caused the sharpening of the peaks associated with the hydride protons of **2** and **7**. A mixture of **2**, **7**, and **4** in the ratio 2:1:7 was observed. After 24 h at room temperature the ^{1}H NMR spectrum, run at −80 °C, revealed that **4** was the only species in solution.

The NMR data described are consistent with the establishment of equilibrium between **2** and **7** as indicated in eq 1. The exchange process is slow at −80 °C, and at −10 °C the rate of the exchange is such that the two hydride resonances collapse. The rate exchange for the process was determined as 0.48 s^{-1} at −70 °C and 0.19 s^{-1} at −80 °C. Above 10 °C decomposition of **7** into **4** starts to take place (eq 2). This reaction led to the formation of H_2, observable when the solution attained room temperature.

$$[W^+]\begin{matrix}H\\H\end{matrix} \rightleftharpoons [W]{-}H + H^+ \qquad (1)$$

$$[W^+]\begin{matrix}H\\H\end{matrix} + TfO^- \longrightarrow [W]{-}OTf + H_2 \qquad (2)$$

[W] =

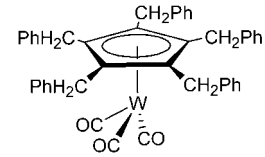

The reactivity pattern observed for complex **2** is similar to that reported by Bullock and co-workers for $[WCp(CO)_3H]$ and $[WCp^*(CO)_3H]$.[10] A noticeable difference between the three hydrides refers to the stability of the corresponding dihydrides $[WCp'(CO)_3(H)_2]^+$ ($Cp' = Cp^{Bz}$, Cp*, Cp), which follows the trend Cp > Cp* > Cp^{Bz}. The ^{1}H NMR spectrum run at −80 °C immediately after addition of 1.2 equiv of HOTf to a CD_2Cl_2 solution of **2** at room temperature revealed the formation of **4** in 49% yield and a total conversion of **2** in 66% yield (**2**:**4**:**7** = 34:49:17). In equivalent conditions, conversion of analogous Cp and Cp* hydrides are 16% and 50%, respectively, thus meaning that the basicity of $[WCp'(CO)_3H]$ increases in the sequence Cp < Cp* < Cp^{Bz}.

Addition of HOTf to a CD_2Cl_2 solution of $[MoCp^{Bz}(CO)_3H]$ (**1**) at −80 °C, as described for the tungsten analogue, led to the immediate formation of $[MoCp(CO)_3OTf]$ (**3**), revealing that the stability of $[MoCp^{Bz}(CO)_3(H)_2]^+$ hampers its detection and the transformation represented in eq 2 prevails despite the temperature.[26] Nevertheless, treatment of a dichloromethane-d_2 solution of **1** with triflic acid in the presence of 1 equiv of 3-pentanone revealed the formation of **3** and a new species that was identified by NMR as the alcohol derivative $[MoCp^{Bz}(CO)_3(Et_2CHOH)]OTf$ (**8**). Characteristic NMR data for **8** at −10 °C are observed at δ 3.79 (CH_2Ph), 3.02 (m, C*H*), 1.67 (multiplet, br., CH_2), and 0.96 ppm (t, CH_3) in the proton spectrum and at δ 90.6 (*C*H), 31.9 (CH_2Ph), 27.6 (CH_2), and 9.6 ppm (CH_3) in the carbon spectrum. During this time, as the temperature is raised from −80 to 0 °C, **1** is completely converted into **3** and **8** in a 1:4 ratio. Further heating to room temperature revealed that ketone conversion attained 73% and that **3** was now the major complex in solution (**3**:**8** = 5:1). This result shows that the competition toward metal coordination between the alcohol and triflate favors the anion coordination and is also consistent with the lack of reactivity between **3** and 3-pentanone. However, in the presence of a more poorly coordinating anion such as BF_4^-, hydride elimination from **1** in the presence of 3-pentanone led to the synthesis of $[MoCp^{Bz}(CO)_3(O{=}CEt_2)]BF_4$ (**9**), which was isolated as a pink

(23) Crabtree, R. H.; Lavin, M.; Bonneviot, L. *J. Am. Chem. Soc.* **1986**, *108*, 4032–4037.

(24) Crabtree, R. H.; Lavin, M. *J. Chem. Soc., Chem. Commun.* **1985**, 1661–1662.

(25) Desrosiers, P. J.; Cai, L. H.; Lin, Z. R.; Richards, R.; Halpern, J. *J. Am. Chem. Soc.* **1991**, *113*, 4173–4184.

(26) Quadrelli, E. A.; Kraatz, H. B.; Poli, R. *Inorg. Chem.* **1996**, *35*, 5154–5162.

solid in 80% yield. The NMR spectra of **9** in CD_2Cl_2 show that the ketone is labile and its dissociation gives rise to the formation of two new species identified as the dichloromethane adduct $[MoCp^{Bz}(CO)_3(CH_2Cl_2)]BF_4$ (**10**) and $[MoCp^{Bz}(CO)_3(FBF_3)]$ (**11**), which exist in solution in a 1:3 ratio. At −80 °C the proton NMR spectrum displays, in addition to characteristic resonances due to the Cp^{Bz} ligand, a broad resonance at δ 5.37 ppm that presents NOE coupling with the aromatic ortho benzyl protons and is due to metal-bonded dichloromethane in **10**. The ^{19}F NMR spectrum at room temperature consists of two resonances at δ −149.92 (br, free BF_4^-) and −156.10 ppm (s, $MoBF_4$) that upon cooling at −80 °C splits into a broad quartet (δ −338.24 ppm, Mo*F*BF_3) and two doublets integrated in the ratio 1:4 at δ −153.04 and −152.97 ppm ($^2J_{FF}$ = 93.8 Hz), assigned to the terminal fluorines MoFB*F*$_3$ of the ^{10}B and ^{11}B isotopomers.[27]

Treatment of an acetone solution of **1** with 1 equiv of Ph_3CBF_4 in CH_2Cl_2 led to $[MoCp^{Bz}(CO)_3(O{=}CMe_2)]BF_4$ (**12**). The spectroscopic features of **12** obtained by IR and NMR attest to its similarity to **9**. As described for **9**, **12** also releases ketone and is converted into a mixture of **10** and **11** in CH_2Cl_2 solution. Despite this behavior, it was possible to grow crystals of **12** from a freshly prepared solution in dichloromethane layered with hexane at −20 °C.

Ketone Hydrogenation. The reactions were performed in CD_2Cl_2 and monitored by NMR. Typically, a mixture of $[MoCp'(CO)_{3-n}(PMe_3)_nH]$ (Cp′ = Cp, n = 0; Cp′ = Cp^{Bz}, n = 0, 1), 3-pentanone (10 equiv) and $Ph_3CBAr'_4$ (Ar′ = $C_6H_3(CF_3)_2$; Mo:Ph_3C^+ = 1:1) in CD_2Cl_2 was frozen and evacuated at liquid nitrogen temperature and the tube was filled with H_2 at 1 atm. The mixture was warmed to room temperature and the reaction progress checked by ^1H NMR. Slow hydrogenation of 3-pentanone proceeds along the time as shown in Figure 1, which also displays the results obtained using $[MoCp(CO)_2(PMe_3)H]$ as the catalyst precursor reported by Bullock and co-workers for comparison.[14] The catalytic activity of $[MoCp^{Bz}(CO)_3H]$ (**1**) is higher than that displayed by all other complexes, and $[MoCp(CO)_3H]$ is the less active compound. The complexes $[MoCp'(CO)_2(PMe_3)H]$ (Cp′ = Cp, Cp^{Bz}) show similar activities, and moreover, Figure 1 shows that they give rise to catalytic systems which deactivate slowly than **1**.

DFT Calculations. The mechanism of the catalytic hydrogenation of acetone to isopropyl alcohol was investigated by means of DFT calculations.[20] In the model used for this study, the catalyst active species, $[MoCp(CO)_3]^+$, corresponds to the metal fragment with the simplest π ligand, i.e., plain cyclopentadienide, for computational expediency. The catalyst with Cp^{Bz}, $[Mo(Cp^{Bz})(CO)_3]^+$, is used for a comparative study of relevant parts of the calculated mechanism (see below). The free energy profile calculated for the reaction is represented in Figure 2.

Coordination of H_2 to the metallic fragment $[MoCp(CO)_3]^+$ results in a 22.0 kcal/mol stabilization of the system, reflecting the electron-deficient character of the metal in the initial complex, a 16-electron species. This is a barrierless process, since no transition state could be located for the addition of hydrogen, at the theory level employed. In the resulting product, $[MoCp(CO)_3(H_2)]^+$ (**A**), formally an 18-electron species, there is an "upright" arrangement of the H_2 fragment, with the MoHH plane perpendicular to the plane of the Cp ring. In **A**, the H−H bond is short (0.848 Å) and strong, as demonstrated by a Wiberg index (WI)[28,29] of 0.604. These values can be compared with the corresponding ones in free H_2 (d = 0.744 Å, WI = 1.000), providing a clear indication of a complex with coordinated dihydrogen, rather than a dihydride species.

The first step in the mechanism corresponds to the breaking of the H−H bond in **A**, yielding a dihydride complex (**B**), as indicated by a large H−H separation (1.864 Å) as well as by the small Wiberg index associated with that interaction (WI = 0.060), precluding the existence of an H−H bond. This is an oxidative addition process, going from Mo(II) in **A** to Mo(IV) in **B**. The corresponding transition state ($\mathbf{TS_{AB}}$) has an intermediate structure, between **A** and **B**. In $\mathbf{TS_{AB}}$, there is a weak H−H interaction (d = 1.278 Å, WI = 0.237), indicating that the process of bond breaking is halfway through when the transition state is reached. The two isomers, **A** and **B**, are equally stable, in practical terms (ΔG = 0.1 kcal/mol), and the low activation energy ($\Delta G^{\ddagger}$ = 3.2 kcal/mol) calculated for the oxidative addition shows a facile process. It should be noted that a mechanism starting directly from the dihydrogen complex (**A**) and not involving **B** was thoroughly investigated. In all cases, the first step corresponds to the formation of dihydride species (**B**), as indicated in Figure 2.

Acetone addition to **B** originates **C**, a complex with a hydrogen interaction between the hydride opposite to the Cp in the metallic fragment, and the O atom of acetone (d_{O-H} = 1.765 Å). The metal hydride that interacts with acetone is determined by electronic factors. In fact, the two hydride ligands in **B** are not equivalent. The H atom opposite to the Cp ligand is considerably electron poorer than the hydride closer to Cp, as shown by the corresponding atomic charges derived from a natural population analysis (NPA):[30−37] 0.19 and 0.11, respectively. Thus, the O atom of an incoming acetone molecule approaches the more positive hydride in **B**: that is, the more acidic MoH bond. Formation of **C** from free acetone and the dihydride complex, **B**, is favorable (ΔG = −3.3 kcal/mol), from a thermodynamic point of view.

The following step, from **C** to **D**, corresponds to H transfer from Mo to the acetone O atom, or, in other words, to protonation of acetone. In the product, **D**, there are two molecular units connected together by a Mo−HO interaction (d_{Mo-H} = 2.604 Å): one can formally be viewed as a neutral monohydride complex and the other is protonated acetone, $[MoCp(CO)_3H]{-}(CH_3)_2COH^+$. Thus, this process corresponds to a reductive elimination step, bringing the metal back to Mo(II). The corresponding transition sate ($\mathbf{TS_{CD}}$) is a rather early one, with the Mo−H bond still far from broken, presenting values of bond length and Wiberg index (d_{Mo-H} = 1.834 Å, WI = 0.400) not far from those of intermediate **C** (d_{Mo-H} = 1.768 Å, WI = 0.454). On the other hand, formation of the

(27) Namorado, S.; Antunes, M. A.; Azevedo, C. G.; Duarte, M. T.; Ascenso, J. R.; Lemos, M. A.; Martins, A. M. Manuscript (containing full details for complexes **10** and **11**) in preparation. See also ref 12.

(28) Wiberg, K. B. *Tetrahedron* **1968**, *24*, 1083–1096.

(29) Wiberg indices are electronic parameters related to the electron density between atoms. They can be obtained from a natural population analysis and provide an indication of the bond strength.

(30) Carpenter, J. E.; Weinhold, F. *J. Mol. Struct. (THEOCHEM)* **1988**, *46*, 41–62.

(31) Carpenter, J. E. Ph.D. Thesis, University of Wisconsin, Madison, WI, 1987.

(32) Foster, J. P.; Weinhold, F. *J. Am. Chem. Soc.* **1980**, *102*, 7211–7218.

(33) Reed, A. E.; Weinhold, F. *J. Chem. Phys.* **1983**, *78*, 4066–4073.

(34) Reed, A. E.; Weinhold, F. *J. Chem. Phys.* **1985**, *83*, 1736–1740.

(35) Reed, A. E.; Weinstock, R. B.; Weinhold, F. *J. Chem. Phys.* **1985**, *83*, 735–746.

(36) Reed, A. E.; Curtiss, L. A.; Weinhold, F. *Chem. Rev.* **1988**, *88*, 899–926.

(37) Weinhold, F.; Carpenter, J. E. *The Structure of Small Molecules and Ions*; Plenum: New York, 1988; p 227

new O−H bond is only incipient in $\mathbf{TS_{CD}}$, with a long distance (1.592 Å), denoting a weak interaction (WI = 0.174), still far from what is observed in **D**, where formation of the O−H bond is completed (d_{O-H} = 1.018 Å, WI = 0.558). A clear positive charge (0.278) calculated for the transferring H atom, in $\mathbf{TS_{CD}}$, confirms this as a protonation step. Acetone protonation, from **C** to **D**, is a favorable process ($\Delta G = -6.6$ kcal/mol) with a negligible activation free energy of 1.3 kcal/mol.

From **D**, reorientation of the protonated acetone with respect to the metallic fragment brings the OH group to the proximity of one CO ligand in the complex, establishing a classical H bond, in **E**, with a O−HO separation of 1.506 Å. This process causes a stabilization of 3.1 kcal/mol, and thus, the system continues to go downhill in terms of free energy. The low value of the activation free energy associated (2.8 kcal/mol) indicates a facile rearrangement.

The following step, from **E** to **F**, represents H transfer from Mo to the C atom of the acetone carbonyl group. In this step the reaction goes from an H-bonded complex between two molecular units, protonated acetone and the monohydride complex [MoCp(CO)$_3$H], in **E**, to a single molecule in **F**. This intermediate (**F**) corresponds to a Mo complex with a molecule of isopropyl alcohol coordinated by the C−H bond of the secondary C atom, $[MoCp(CO)_3\{(CH_3)_2CHOH\}]^+$. In the corresponding transition state ($\mathbf{TS_{EF}}$), formation of the new C−H bond is only incipient (d_{C-H} = 1.842 Å, WI = 0.170), while Mo−H bond breaking is just starting, as shown by a separation of 1.764 Å and a Wiberg index of 0.457, values not far from those of intermediate **E** (d_{Mo-H} = 1.704 Å, WI = 0.536). The H-transfer process from **E** to **F** corresponds, in fact, to hydride transfer from the metal to the C atom of the carbonyl group in protonated acetone, as demonstrated by a negative charge calculated for the transferring H atom in $\mathbf{TS_{EF}}$ (−0.026). This step is slightly unfavorable ($\Delta G = 0.2$ kcal/mol), and the corresponding activation free energy (7.4 kcal/mol), although reachable, presents the highest value for the reaction, from the aggregate between acetone and the dihydride complex (**C**) to the complex with O-coordinated isopropyl alcohol (**G**).

The final step of the mechanism, from **F** to **G**, is a rearrangement of isopropyl alcohol in the coordination sphere of the metal. The system goes from a coordination established by the C−H bond of the central C atom, in **F**, to O coordination in the product, **G**. In the transition state, $\mathbf{TS_{FG}}$, the structure is intermediate between the two minima involved, **F** and **G**. In $\mathbf{TS_{FG}}$, the Mo−H bond is practically broken (d_{Mo-H} = 2.218 Å, WI = 0.058), while formation of the new Mo−O bond is only beginning with values of bond distance (2.955 Å) and Wiberg index (0.040) far from the ones found in the product, **G** (d_{Mo-O} = 2.242 Å, WI = 0.299). This step is very favorable, from a thermodynamic point of view ($\Delta G = -17.3$ kcal/mol), and the activation free energy calculated (4.4 kcal/mol) is accessible.

The energy profile calculated for the reaction (Figure 2) shows that, overall, the system goes downhill, in free energy terms, from the initial aggregate between acetone and the dihydride complex (**C**) until **G**, the complex with isopropyl alcohol coordinated through the O atom. In fact, an energy variation of $\Delta G = -26.8$ kcal/mol is associated with that process, from **C** to **G**, corresponding to an exergonic reaction and indicating the stability of the product, with respect to the reagent. In addition, coordination of one molecule of acetone (one of the reagents) to the metal center is a competitive process, since the reaction of ligand exchange from isopropyl alcohol, in **G**, to acetone, in **H**, is exergonic ($\Delta G = -3.7$ kcal/mol; see Figure 2). The

Scheme 2. Comparative Reactivity of the Isopropyl Alcohol Complex with Cp and Cp^{Bz} as Coligands[36]

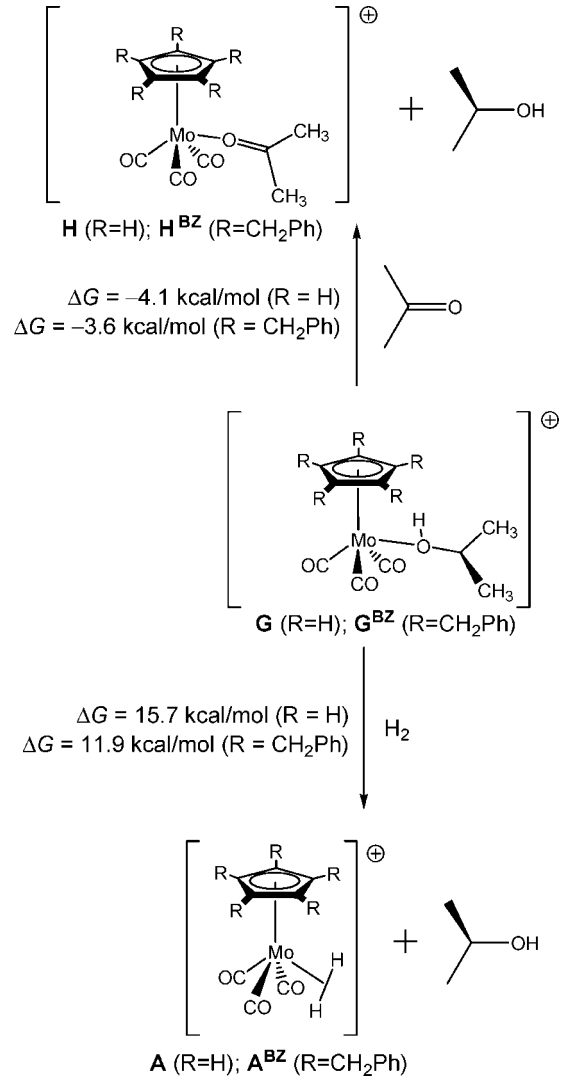

stabilities of the complexes with coordinated isopropyl alcohol (**G**) and with coordinated acetone (**H**) are most probably the major drawbacks of this system with respect to catalysis, since an overstabilization of those species means that both the reaction product and the reagent are, at least partially, blocking the metal coordination position and, thus, the catalytic site. This effect is reflected in the closure of the catalytic cycle, that is, regeneration of the dihydrogen complex (**A**) from **H**, releasing one molecule of acetone and coordinating one molecule of H_2. The energy variation associated with that process, from **H** back to **A** ($\Delta G = 12.0$ kcal/mol; see Figure 2), is higher than any energy barrier calculated for the elementary steps of the mechanism, thus corresponding to the rate-limiting step of the entire process and explaining the poor performance of the Cp complex as a catalyst for the reaction, as experimentally observed.

Key features of the catalytic reaction with the pentabenzylcyclopentadienyl (Cp^{Bz}) complex as catalyst were also investigated computationally, for comparison purposes. Thus, regeneration of the dihydrogen complex $[MoCp^{Bz}(CO)_3(H_2)]^+$ ($\mathbf{A^{Bz}}$) from the acetone complex $[MoCp^{Bz}(CO)_3(O{=}CMe_2)]^+$ ($\mathbf{H^{Bz}}$) is less unfavorable than the equivalent process for the Cp system, with an energy variation 4.2 kcal/mol lower (see Scheme 2).[38]

(38) Energy values obtained for the gas phase at the PBE1PBE/b1 level (see Computational Details).

This corresponds to the rate-limiting step of the catalytic cycle (see above), and thus, a lower energy cost associated with the Cp^{Bz} catalyst suggests that this should be a better catalyst than the Cp system, in good accord with the experimental observations. An increased steric bulk of Cp^{Bz}, when compared with Cp, destabilizes the coordination of acetone in $\mathbf{H^{Bz}}$. Accordingly, acetone coordination is weaker in the Cp^{Bz} complex than in the Cp analogue, as shown by a longer bond length (2.234 and 2.202 Å in $\mathbf{H^{Bz}}$ and **H**, respectively) and the associated Wiberg indices (0.307 in $\mathbf{H^{Bz}}$ and 0.333 in **H**). Interestingly, the ligand exchange process, switching of isopropyl alcohol and acetone (from **G** to **H** and from $\mathbf{G^{Bz}}$ to $\mathbf{H^{Bz}}$), has similar energy variations in both systems (within 0.5 kcal/mol;[38] see Scheme 2) since the two ligands have equivalent steric requirements.

The highest energy barrier calculated for the consecutive steps of the hydrogenation reaction (from **C** to **G**) corresponds to hydride transfer from the metal center to protonated acetone, from **E** to **F** in the path calculated for the Cp catalyst, represented in Figure 2. This step was also calculated for the Cp^{Bz} catalyst (see Figure S1 in the Supporting Information). The general features of the process are equivalent for both catalysts and, thus, a detailed discussion is unnecessary, but some aspects deserve further notice. The first is the negative charge (−0.023) calculated for the transferring H atom in the transition state ($\mathbf{TS_{EF}^{Bz}}$), indicative of a hydride nature, similarly to what happens in $\mathbf{TS_{EF}}$ with the Cp catalyst, discussed above. The second result is a slightly lower activation free energy calculated for hydride transfer with the Cp^{Bz} catalyst, in comparison with that obtained for the Cp system. This indicates that hydride transfer is favored for the Cp^{Bz} system, resulting from the presence of a better electron donor (Cp^{Bz} vs Cp). Finally, a difference of less than 2 kcal/mol was obtained[38] for the energy barriers of hydride transfer calculated in the gas phase, on comparing the two catalysts (with Cp^{Bz} and with Cp), suggesting that the model used for the mechanistic investigations, $[MoCp(CO)_3]^+$, provides a good description of the system.

Crystallographic Studies. Crystals of **3**, **4**, and **12** suitable for X-ray diffraction structure determinations have been obtained from diethyl ether (**3** and **4**) and CH_2Cl_2/hexane (**12**) at −20 °C. Complexes **3** and **4** crystallize in the monoclinic space group $P2_1/c$, and **12** crystallizes in the triclinic space group $P\bar{1}$ with two independent molecules in the unit cell. The molecular structures are shown in Figures 3− and 5, and selected bond distances and angles are shown in Table 2 (only one set of data are shown for **12**).

In all complexes the metal coordination geometry can be best described as a distorted four-legged piano stool with Cp^{Bz}-(CT)−M−O(4) angles of 109.79(9), 109.45(18), and 104.84(13)° for **3**, **4**, and **12**, respectively, and Cp^{Bz}(CT)−M−C(*i*) (*i* = 6, 7, 8) angles in the ranges 108.4−128.9° for **3** and **4** and 107.7−124.0° for **12** (Cp^{Bz}(CT) = centroid of the cyclopentadienyl ring). The spatial arrangements of the cyclopentadienyl substituents in all compounds exhibit four benzyl aromatic groups opposite to the metal and one bent down toward it, although, as expected for 18-electron complexes, sufficiently far apart to prevent any bonding interaction. The relative conformation of the phenyl rings may be characterized by the torsion angles defined by M−C(Cp^{Bz})−C(CH_2)−C_{ipso} (see the Supporting Information). The arrangement observed in **3**, **4**, and **12** is analogous to that observed for other MCp^{Bz} (M = Mo(II), W(II)) complexes previously reported.[17,19] The M−Cp^{Bz}(CT) and the M−C(*i*) (*i* = 1−5) bond distances are comparable to the values determined for other pentabenzylcyclopentadienyl complexes,[17−19] and the M−C and C−O bond distances as well as the M−C−O angles are typical for terminal carbonyl ligands. The M−O(4) distances in **3** and **4** are close to the value of 2.212(2) Å reported for $[MoCp(CO)_3OTf]$[39] and slightly longer than the M−O(4) distance in **12**, reflecting the usual difference between neutral and anionic metal−oxygen bond lengths.[40] The carbonyl carbon of the coordinated ketone in **12** is planar, consistent with sp^2 character. The methyl groups of the ketone ligand are almost perpendicular to the cyclopentadienyl ring plane (86.56(5)°) and coplanar with the CO ligand in a trans position. Interestingly, the structure optimized for **12** by means of DFT calculations (corresponding to $\mathbf{H^{Bz}}$), is in excellent agreement with the X-ray structure, reproducing all conformational arrangements discussed above: namely, the "upright" conformation of coordinate acetone, perpendicular to Cp^{Bz}, and the spacial arrangement of the substituents in the cyclopentadienyl ring. In addition, the calculated bond distances (Mo−C_{CO} = 2.00−2.01 Å, Mo−O_{acet} = 2.23 Å, and Mo−Cp^{Bz}(CT) = 2.01 Å) compare well with the experimental values (see Table 2). These results show that the theoretical method used in the

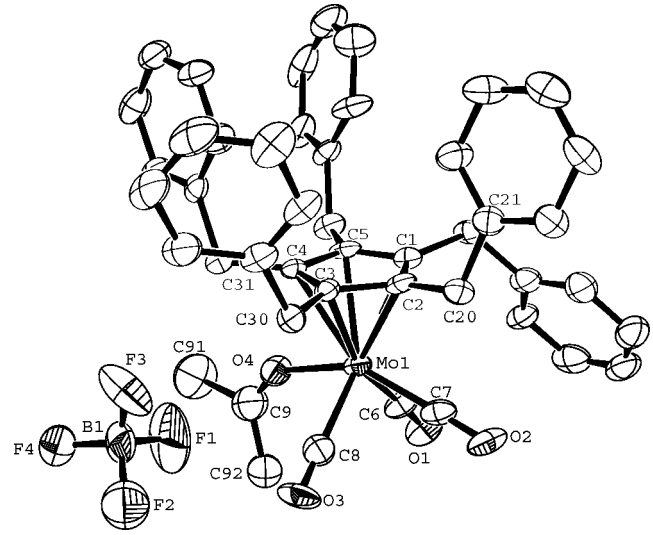

Figure 5. Molecular structure of **12** showing thermal ellipsoids at the 50% probability level. Hydrogen atoms are omitted for clarity.

Table 2. Selected Bond Lengths (Å) and Angles (deg) for 3, 4, and 12

	$[MoCp^{Bz}(CO)_3OTf]$ (**3**)	$[WCp^{Bz}(CO)_3OTf]$ (**4**)	$[MoCp^{Bz}(CO)_3(OCMe_2)]BF_4$ (**12**)
M−Cp^{Bz}(CT)	2.0004(4)	1.9984(4)	2.0245(8)
M−C(6)	2.006(5)	2.074(12)	2.032(9)
M−C(7)	1.994(4)	1.981(10)	1.973(9)
M−C(8)	2.057(5)	2.011(12)	2.037(9)
C(6)−O(1)	1.131(6)	1.120(12)	1.125(9)
C(7)−O(2)	1.135(5)	1.148(11)	1.149(9)
C(8)−O(3)	1.139(6)	1.135(13)	1.119(9)
M−O(4)	2.187(3)	2.174(6)	2.156(5)
C(9)−S(1)/O(4)	1.828(5)	1.799(12)	1.169(11)
M−C(6)−O(1)	173.1(5)	176.5(9)	176.0(7)
M−C(7)−O(2)	179.6(4)	178.9(8)	178.1(7)
M−C(8)−O(3)	177.0(4)	172.7(9)	172.9(7)
M−O(4)−S(1)/C(9)	140.5(2)	138.3(5)	144.8(7)

(39) Lindner, E.; Henes, M.; Wielandt, W.; Eichele, K.; Steimann, M.; Luinstra, G. A.; Gortz, H.-H. *J. Organomet. Chem.* **2003**, *681*, 12–13.
(40) Orpen, A. G.; Brammer, L.; Allen, F. H.; Kennard, O.; Watson, D. G.; Taylor, R. *J. Chem. Soc., Dalton Trans.* **1989**, S1–S83.

Scheme 3. Catalytic Cycle for Ketone Hydrogenation

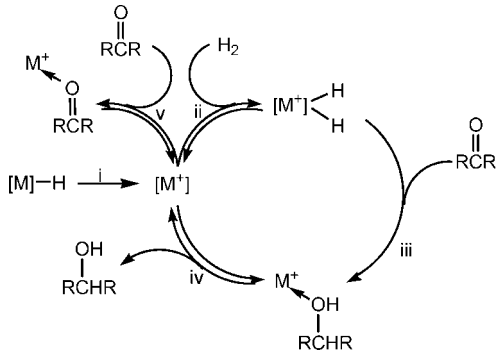

mechanistic studies provides a good description of the system, from a structural point of view. Short intermolecular contacts were found in **3**, **4**, and **12.** In **12** each anion interacts with two cations in the asymmetric unit, displaying hydrogen bonds of the type F···H−C, ranging from 2.401(9) to 2.769(9) Å (see Figure S2 in the Supporting Information).

Conclusion

Scheme 3 shows a catalytic cycle for the hydrogenation of ketones with $[MoCp(CO)_3(H)_2]^+$. According to the calculated mechanism, the catalytic reaction depends on a balance between the acidity of the Mo(IV) dihydride, $[MoCp(CO)_3(H)_2]^+$, the hydricity of Mo(II) hydride species, $[MoCp(CO)_3H]$, and the stability of $[MoCp(CO)_3L]^+$ cations (L = acetone, isopropyl alcohol). The higher activity displayed by $[MoCp^{Bz}(CO)_3H]$ in comparison with that of the Cp analogue may be envisaged as a consequence of the higher steric constraint created by the Cp^{Bz} ligand compared to Cp and the consequent destabilization of the species $[MoCp'(CO)_3L]^+$ (L = ketone, alcohol) with the steric bulk of the Cp′ ligand. As a consequence, blocking of hydrogen activation by the ketone or the alcohol (iv and v in Scheme 3) is less effective in the case of $[MoCp^{Bz}(CO)_3]^+$, making this complex a better catalyst. The lability of the alcohol and ketone ligands revealed by the NMR results of **8**, **9**, and **12** is consistent with this assumption. Moreover, the preferred orientation of the ketone ligand in **12** is a further argument to justify the lower stability of the $[MoCp^{Bz}(CO)_3(ketone)]^+$ cation in comparison with its Cp analogue. The much lower activity of $[MoCp(CO)_3H]$ most probably reflects the stability of the species $[MoCp(CO)_3L]^+$ that constitute deactivation pathways of the catalytic system if dissociation of L does not take place. This reasoning is also consistent with the results reported for the hydrogenation activity of $[MoCp(CO)_2(PR_3)H]$ (R = Me, Ph, Cy), which increases with the phosphine cone angle.[14] The better catalytic performance of $[MoCp^{Bz}(CO)_3H]$ in comparison with Cp or Cp^{Bz} dicarbonyl phosphine analogues must also be a reflection of the higher stability of that catalyst, which is not prone to ligand protonation.

Experimental Section

General Procedures. All operations were performed under a dry nitrogen atmosphere using standard Schlenk and glovebox techniques. Solvents were previously dried with 4 Å molecular sieves and distilled under a dry nitrogen atmosphere over CaH_2 (dichloromethane and hexane) or sodium/benzophenone (diethyl ether and toluene). Dichloromethane-d_2 and toluene-d_8 were dried with 4 Å molecular sieves, degassed, and stored under dry nitrogen. HCp^{Bz},[21] $[MoCp^{Bz}(CO)_3H]$,[19] $[WCp^{Bz}(CO)_3H]$],[19] $[MoCp^{Bz}(CO)_3Me]$,[17] $[WCp^{Bz}(CO)_3Me]$,[17] and $Ph_3CBAr'_4$[41] were prepared according to methods described in the literature. Triflic acid and Ph_3CBF_4 were used as received from Aldrich. NMR spectra were recorded on Bruker Avance^{II} 300 and Bruker Avance^{II} 400 spectrometers. Chemical shifts for ^1H were referenced to resonances of the residual protonated solvents relative to tetramethylsilane, and ^{13}C spectra were referenced to the solvent carbon resonance. ^{19}F spectra were referenced to external CF_3COOH (δ −76.55 ppm). ^{11}B spectra were referenced to external $BF_3 \cdot Et_2O$ (δ 0 ppm). IR spectra were recorded as KBr pellets on a Jasco FI/IR-4100 spectrometer. Elemental analyses were performed at the Laboratório de Análises do IST, Lisbon, Portugal.

$[MoCp^{Bz}(CO)_3OTf]$ (3). A solution of triflic acid (45 μL, 0.50 mmol) in dichloromethane (5 mL) was added dropwise, at room temperature, to a solution of $[MoCp^{Bz}(CO)_3H]$ (0.340 g, 0.50 mmol) (15 mL) in the same solvent. The color of the mixture changed immediately from pale yellow to dark red. The solution was stirred for $^1/_2$ h. The solvent was evaporated under vacuum, and the red residue obtained was extracted in diethyl ether and the extract filtered. Concentration and cooling to −20 °C yielded red crystals (0.398 g, 0.47 mmol, yield 94%). ^1H NMR (CD_2Cl_2): δ 7.15−7.08 (m, 15 H, *p*-C_6H_5, *m*-C_6H_5), 6.84−6.81 (m, 10 H, *o*-C_6H_5), 3.73 (s, 10 H, CH_2Ph). ^{13}C NMR (CD_2Cl_2): δ 243.9 (*CO trans* OTf), 225.5 (*CO*), 138.0 (*i*-C_6H_5), 129.0 (*o*-C_6H_5), 128.9 (*m*-C_6H_5), 127.4 (*p*-C_6H_5), 117.4 (C_5Bz_5), 32.4 (CH_2Ph). ^{19}F NMR (CD_2Cl_2): δ −77.4 (s, CF_3SO_3). ^1H NMR (toluene-d_8): δ 6.86−6.84 (m, 15 H, *p*-C_6H_5, *m*-C_6H_5), 6.60−6.57 (m, 10 H, *o*-C_6H_5), 3.54 (s, 10 H, CH_2Ph). ^{13}C NMR (toluene-d_8): δ 244.9 (*CO trans* OTf), 225.5 (*CO*), 137.5 (*i*-C_6H_5), 128.9 (*o*-C_6H_5), 128.7 (*m*-C_6H_5), 127.2 (*p*-C_6H_5), 117.1 (C_5Bz_5), 32.2 (CH_2Ph). ^{19}F NMR (toluene-d_8): δ −73.4 (s, CF_3SO_3). IR (KBr pellet): $\nu_{C\equiv O}$ 2058, 1981, 1956 cm^{-1}; $\nu_{as}(SO_3)$ 1336, 1196 cm^{-1}; $\nu_s(SO_3)$ 1014 cm^{-1}. Anal. Calcd for $C_{44}H_{35}O_6F_3MoS$: C, 62.40; H, 4.17. Found: C, 62.61; H, 4.04.

$[WCp^{Bz}(CO)_3OTf]$ (4). Method 1. A solution of triflic acid (45 μL, 0.5 mmol) in dichloromethane (10 mL) was added dropwise, at room temperature, to a solution of $[WCp^{Bz}(CO)_3H]$ (0.392 g, 0.50 mmol) in dichloromethane (20 mL). A color change from pale yellow to dark orange was observed. The mixture was stirred for $^1/_2$ h. The solvent was evaporated under vacuum, and the orange residue obtained was extracted in diethyl ether and the extract filtered. Concentration of the solution and cooling to −20 °C yielded a microcrystalline orange solid (0.429 g, 0.46 mmol, yield 92%).

Method 2. A solution of triflic acid (29 μL, 0.33 mmol) in dichloromethane was added dropwise, at −50 °C, to a solution of $[WCp^{Bz}(CO)_3Me]$ (0.263 g, 0.33 mmol) in dichloromethane. The mixture was slowly warmed to room temperature, and a color change from yellow to dark orange was observed. The mixture was stirred for 1.5 h at room temperature. Removal of the solvent under vacuum resulted in the formation of an orange solid that was extracted in diethyl ether; the extract was filtered, concentrated, and cooled to −20 °C to afford orange crystals (0.285 g, 0.31 mmol, yield 92%). ^1H NMR (CD_2Cl_2): δ 7.15−7.07 (m, 15 H, *p*-C_6H_5, *m*-C_6H_5), 6.84−6.81 (m, 10 H, *o*-C_6H_5), 3.80 (s, 10 H, CH_2Ph). ^{13}C NMR (CD_2Cl_2): δ 234.0 (*CO trans* OTf), 220.1 (*CO*), 138.1 (*i*-C_6H_5), 129.0 (*o*-C_6H_5), 128.9 (*m*-C_6H_5), 127.4 (*p*-C_6H_5), 114.9 (C_5Bz_5), 32.6 (CH_2Ph). ^{19}F NMR (CD_2Cl_2): δ −76.8 (s, CF_3SO_3). IR (KBr pellet): $\nu_{C\equiv O}$ 2050, 1968, 1947 cm^{-1}; $\nu_{as}(SO_3)$ 1346, 1195 cm^{-1}; $\nu_s(SO_3)$ 1009 cm^{-1}. Anal. Calcd for $C_{44}H_{35}O_6F_3WS$: C, 56.64; H, 3.78; S, 3.44. Found: C, 57.38; H, 4.09; S, 3.44.

Protonation of $[WCp^{Bz}(CO)_3H]$ To Give $[WCp^{Bz}(CO)_3(H)_2]OTf$ (7). In an NMR tube containing a frozen solution of triflic acid (5 μL, 0.05 mmol) in CD_2Cl_2 a CD_2Cl_2 solution of $[WCp^{Bz}(CO)_3H]$ (0,024 mg, 0.03 mmol) was added, and the tube was sealed. The tube was placed in a bath at −80 °C and the mixture stirred. The NMR spectra run at −80 °C showed the formation of

(41) Bahr, S. R.; Boudjouk, P. *J. Org. Chem.* **1992**, *57*, 5545–5547.

Table 3. Crystallographic Data for 3, 4, and 12

	$[MoCp^{Bz}(CO)_3OTf]$ (**3**)	$[WCp^{Bz}(CO)_3OTf]$ (**4**)	$[MoCp^{Bz}(CO)_3(OCMe_2)]BF_4$ (**12**)
formula	$C_{44}H_{35}F_3O_6SMo \cdot {}^1/_4Et_2O$	$C_{44}H_{35}F_3O_6SW \cdot {}^1/_4Et_2O$	$C_{46}H_{41}BF_4O_4Mo$
formula wt	854.01	941.91	840.54
temp (K)	150(2)	150(2)	150(2)
wavelength (Å)	0.710 73	0.710 73	0.710 69
cryst syst	monoclinic	monoclinic	triclinic
space group	$P2_1/c$	$P2_1/c$	$P\bar{1}$
unit cell dimens			
a (Å)	10.0960(19)	10.0710(7)	12.661(5)
b (Å)	17.894(4)	17.8840(12)	15.214(5)
c (Å)	22.843(5)	22.7960(16)	21.710(7)
α (deg)			83.015(18)
β (deg)	98.102(6)	97.901(4)	89.04(2)
γ (deg)			89.57(2)
V (Å^3)	4085.6(14)	4066.8(5)	4150(2)
Z	4	4	2
calcd density (Mg/m^3)	1.373	1.523	1.345
abd coeff (mm^{-1})	0.432	2.952	0.376
F(000)	1728	1856	1728
cryst size (mm)	0.40 × 0.15 × 0.15	0.30 × 0.10 × 0.02	0.24 × 0.18 × 0.04
θ range for data collection (deg)	1.45−27.99	1.45−26.40	0.94−26.51
limiting indices	$-13 \le h \le 13$	$-12 \le h \le 12$	$-15 \le h \le 15$
	$-23 \le k \le 23$	$-21 \le k \le 22$	$-19 \le k \le 18$
	$-30 \le l \le 30$	$-28 \le l \le 28$	$-27 \le l \le 27$
no. of collected/unique rflns	85 319/9803 (R_{int} = 0.0706)	74 326/8317 (R_{int} = 0.1398)	45 230/16 918 (R_{int} = 0.0997)
completeness to θ (%)	99.5 (θ = 27.99°)	99.5 (θ = 26.40°)	98.3 (θ = 26.51°)
abs cor	multiscan	multiscan	multiscan
refinement method	full-matrix least squares on F^2	full-matrix least squares on F^2	full-matrix least squares on F^2
no. of data/restraints/params	9803/2/520	8317/2/505	16 918/0/1009
goodness of fit on F^2	1.093	1.081	0.940
final R indices ($I > 2\sigma(I)$)	R1 = 0.0563, wR2 = 0.1744	R1 = 0.0523, wR2 = 0.1296	R1 = 0.0787, wR2 = 0.1825
R indices (all data)	R1 = 0.0802, wR2 = 0.2068	R1 = 0.1126, wR2 = 0.1737	R1 = 0.1707, wR2 = 0.2114
largest diff peak, hole (e Å^{-3})	1.791, −1.295	1.979, −1.893	0.589, −0.851

7 in 50% yield. ^{1}H NMR (CD_2Cl_2, −70 °C): δ 7.17−7.06 (m, 15 H, *p*-C_6H_5, *m*-C_6H_5), 6.80−6.76 (m, 10 H, *o*-C_6H_5), 3.89 (s, 10 H, CH_2Ph), −1.96 (s, 2 H, W(H)$_2$). ^{13}C NMR (CD_2Cl_2, −70 °C): δ 215.9 (*C*O), 193.2 (*C*O *cis* WH_2), 136.0 (*i*-C_6H_5), 128.7 (*o*-C_6H_5), 127.7 (*m*-C_6H_5), 127.4 (*p*-C_6H_5), 120.1−115.9 (*C*F_3), 110.2 (C_5Bz_5), 30.6 (*C*H_2Ph). ^{19}F NMR (CD_2Cl_2, −70 °C): δ −0.48 (s, CF_3SO_3). T_1 and k_D values (300 MHz, CD_2Cl_2): −80 °C, T_1 = 498 ms, k_D = 0.19 s^{-1}; −70 °C, T_1 = 472 ms, k_D = 0.48 s^{-1}.

Reaction of $[MoCp^{Bz}(CO)_3H]$ (1) with Triflic Acid in the Presence of 3-Pentanone. In an NMR tube, a solution of **1** (25.3 mg, 0.04 mmol) and 3-pentanone (4 μL, 0.04 mmol) in dichloromethane-d_2 was frozen and treated with a solution of triflic acid (3.5 μL, 0.04 mmol) in the same solvent. The tube was sealed, and the reaction was followed by NMR from −50 °C to room temperature. At −50 °C the ^{1}H and ^{13}C spectra revealed the presence of three different molybdenum species that could be identified as compounds **1**, **3**, and $[MoCp^{Bz}(CO)_3(Et_2CHOH)]OTf$ (**8**). The spectra also showed the resonances due to free 3-pentanone (^{1}H NMR (CD_2Cl_2, −50 °C) δ 2.64−2.57 (q, 4 H, $(CH_3CH_2)_2CO$), 1.06−1.01 (t, 6 H, $(CH_3CH_2)_2CO$); ^{13}C NMR (CD_2Cl_2, −50 °C) δ 35.5 ($(CH_3CH_2)_2CO$), 7.5 ($(CH_3CH_2)_2CO$)). ^{1}H NMR (CD_2Cl_2, −50 °C): for **1**, δ 7.11−7.06 (m, 15 H, *p*-C_6H_5, *m*-C_6H_5), 6.85−6.67 (m, 10 H, *o*-C_6H_5), 3.82 (s, 10 H, CH_2Ph), −5.19 (s, 1 H, Mo−H); for **3**, δ 7.11−7.06 (m, 15 H, *p*-C_6H_5, *m*-C_6H_5), 6.85−6.67 (m, 10 H, *o*-C_6H_5), 3.70 (s, 10 H, CH_2Ph); for **8** (CD_2Cl_2, −10 °C), δ 7.08 (m, 15 H, *p*-C_6H_5, *m*-C_6H_5), 6.73 (m, 10 H, *o*-C_6H_5), 3.79 (s, 10 H, CH_2Ph), 3.02 (m, 1 H, $(CH_3CH_2)_2CHOH$), 1.67 (m, 4 H, $(CH_3CH_2)_2CHOH$), 0.96 (t, 6 H, $(CH_3CH_2)_2CHOH$), 0.10 (s, 1 H, $(CH_3CH_2)_2CHOH$). ^{13}C NMR (CD_2Cl_2, −50 °C): δ 244.1, 241.2, 224.8, 222.1 (*C*O), 139.9, 138.0, 137.3 (*i*-C_6H_5), 128.5, 128.3, 128.2, 128.0 (*o,m*-C_6H_5), 126.8, 126.7, 126.0 (*p*-C_6H_5), 121.4−117.1 (q, *C*F_3), 116.4, 116.1, 110.9 (C_5Bz_5), 89.7 ($(CH_3CH_2)_2CHOH$, **8**), 31.7, 31.5, 31.4 (*C*H_2Ph), 27.0 ($(CH_3CH_2)_2CHOH$, **8**), 9.1 ($(CH_3CH_2)_2CHOH$, **8**). ^{13}C NMR data for **8** (CD_2Cl_2, −10 °C): δ 241.7 (*C*O), 228.0 (*C*O), 137.4 (*i*-C_6H_5), 128.7 (*o*-C_6H_5), 128.3 (*m*-C_6H_5), 127.1 (*p*-C_6H_5), 116.6 (C_5Bz_5), 90.6 ($(CH_3CH_2)_2CHOH$), 31.9 (*C*H_2Ph), 27.6 ($(CH_3CH_2)_2CHOH$), 9.6 ($(CH_3CH_2)_2CHOH$). ^{19}F NMR (CD_2Cl_2, −50 °C): δ −76.8 (s, CF_3SO_3).

Reaction of $[MoCp^{Bz}(CO)_3H]$ (1) with $Ph_3CBF_4^-$ in the Presence of 3-Pentanone. Synthesis of $[MoCp^{Bz}(CO)_3(O{=}CEt_2)]BF_4$ (9). A dichloromethane (5 mL) solution of $Ph_3C^+BF_4^-$ (0.144 g, 0.44 mmol) was added to a solution of $[MoCp^{Bz}(CO)_3H]$ (0.304 g, 0.44 mmol) and 3-pentanone (1 mL, 14 mmol) in the same solvent (5 mL). The solution immediately turned red. After the mixture was stirred for 15 min, hexane (20 mL) was added and a precipitate formed. The solid was allowed to settle, and the solution was filtered. The pink microcrystalline solid obtained was dried under vacuum (0.352 g, 0.4 mmol, yield 80%). ^{1}H NMR (CD_2Cl_2, 25 °C): for **9**, δ 7.20−7.00 (m, 15 H, *p*-C_6H_5, *m*-C_6H_5), 6.82−6.68 (m, 10 H, *o*-C_6H_5), 3.82 (s, 10 H, CH_2Ph), 2.74−2.66 (q, 4 H, $(CH_3CH_2)_2C{=}O$), 1.32−1.27 (t, 6 H, $(CH_3CH_2)_2C{=}O$); for **10**, δ 7.20−7.00 (m, 15 H, *p*-C_6H_5, *m*-C_6H_5), 6.82−6.68 (m, 10 H, *o*-C_6H_5), 5.37 (br, MoClCH_2Cl), 3.76 (s, 10 H, CH_2Ph); for **11**, δ 7.20−7.00 (m, 15 H, *p*-C_6H_5, *m*-C_6H_5), 6.82−6.68 (m, 10 H, *o*-C_6H_5), 3.71 (s, 10 H, CH_2Ph). ^{13}C NMR (CD_2Cl_2, 25 °C): δ 240.0, 227.4, 226.5, 225.6 (*C*O), 138.0, 137.8, 137.6 (*i*-C_6H_5), 129.2, 129.0, 128.9 (*o*-C_6H_5), 128.9, 128.7, 128.6 (*m*-C_6H_5), 127.5, 127.3, 127.2 (*p*-C_6H_5), 118.0, 117.7, 117.0 (C_5Bz_5), 54.0 (MoCl*C*H_2Cl, **10**), 38.9 ($(CH_3CH_2)_2C{=}O$, **9**), 32.3, 32.2, 32.1 (*C*H_2Ph), 9.9 ($(CH_3CH_2)_2C{=}O$, **9**). ^{19}F NMR (CD_2Cl_2, −80 °C): δ −150.28 (br, BF_4^-), −152.97 (d, $^2J_{FF}$ = 93.7 Hz, (μ-F)$^{10}BF_3$, **11**), −153.04 (d, $^2J_{FF}$ = 93.8 Hz, (μ-F)$^{11}BF_3$, **11**), −338.24 (q, $^2J_{FF}$ = 92.1 Hz, (μ-*F*)BF_3, **11**). ^{11}B NMR (CD_2Cl_2, 25 °C): δ 0.06 ((μ-F)*B*F_3, **11**), −0.26 (*B*F_4^-). IR (KBr pellet): $\nu_{C\equiv O}$ 2055, 1975, 1954 cm^{-1}; $\nu_{O=CEt_2}$ 1633 cm^{-1}; ν_{BF_4} 1084, 1058, 1029 cm^{-1}. Anal. Calcd for $C_{48}H_{45}O_4F_4MoB$: C, 66.37; H, 5.22. Found: C, 66.38; H, 4.82.

Reaction of $[MoCp^{Bz}(CO)_3H]$ (1) with $Ph_3CBF_4^-$ in the Presence of Acetone. Synthesis of $[MoCp^{Bz}(CO)_3(O{=}CMe_2)]BF_4$ (12). A dichloromethane (5 mL) solution of Ph_3CBF_4 (0.170 g, 0.5 mmol) was added to a solution of $[MoCp^{Bz}(CO)_3H]$ (0.349 g, 0.5 mmol) and acetone (0.2 mL, 2.7 mmol) in the same solvent

(5 mL). The solution immediately turned red. After the mixture was stirred for 15 min, hexane (20 mL) was added and a precipitate formed. The solid was allowed to settle, and the solution was filtered off. The compound was recrystallized at −20 °C from diffusion of hexane into a dichloromethane solution, yielding purple crystals (0.397 g, 0.45 mmol, yield 90%). ^{1}H NMR (CD_2Cl_2, 25 °C): for **12**, δ 7.12−7.04 (m, 15 H, *p*-C_6H_5, *m*-C_6H_5), 6.82−6.77 (m, 10 H, *o*-C_6H_5), 3.80 (s, 10 H, CH_2Ph), 2.53 (s, 6 H, $(CH_3)_2$C=O); for **10**, δ 7.12−7.04 (m, 15 H, *p*-C_6H_5, *m*-C_6H_5), 6.82−6.77 (m, 10 H, *o*-C_6H_5), 5.30 (br, MoClCH_2Cl), 3.76 (s, 10 H, CH_2Ph); for **11**, δ 7.12−7.04 (m, 15 H, *p*-C_6H_5, *m*-C_6H_5), 6.82−6.77 (m, 10 H, *o*-C_6H_5), 3.71 (s, 10 H, CH_2Ph). ^{13}C NMR (CD_2Cl_2, 25 °C): δ 242.3, 240.5, 234.4, 233.7 (*C*O), 226.6 (*C*O, O*C*Me_2, **12**), 226.3, 225.6 (*C*O), 138.0, 137.7, 137.4 (*i*-C_6H_5), 129.2, 129.0, 128.9 (*o*-C_6H_5), 128.9, 128.8, 128.7 (*m*-C_6H_5), 127.4, 127.1 (*p*-C_6H_5), 118.0, 117.8, 117.0 (C_5Bz_5), 54.0 (MoCl*C*H_2Cl, **10**), 34.2 ((CH_3)$_2$C=O, **12**), 32.3, 32.0 (*C*H_2Ph). ^{19}F NMR (CD_2Cl_2, −80 °C): δ −149.82 (br, BF_4^-), −152.96 (d, $^2J_{FF}$ = 93.7 Hz, (μ-F)$^{10}BF_3$, **11**), −153.02 (d, $^2J_{FF}$ = 93.8 Hz, (μ-F)$^{11}BF_3$, **11**), −338.24 (q, $^2J_{FF}$ = 93.6 Hz, (μ-*F*)BF_3, **11**). ^{11}B NMR (CD_2Cl_2, 25 °C): δ 0.49 ((μ-F)*B*F_3, **11**), −0.23 (*B*F_4^-). IR (KBr pellet): $\nu_{C\equiv O}$ 2057, 2036, 1978, 1958 cm^{-1}; $\nu_{O=CMe_2}$ 1657 cm^{-1}; ν_{BF_4} 1056 cm^{-1}. Anal. Calcd for $C_{46}H_{41}O_4F_4MoB\cdot 0.5CH_2Cl_2$: C, 63.11; H, 4.79. Found: C, 63.20; H, 4.49.

Catalytic Hydrogenations. [$MCp^{Bz}(CO)_3H$] (0.0125 mmol) and 1 equiv of $Ph_3CBAr'_4^-$ (0.0125 mmol) were placed in an NMR tube equipped with a J. Young valve, and a solution of 3-pentanone (0.123 mmol) in CD_2Cl_2 (400 μL) was added. Under these conditions the concentration of catalyst is 30 mM and the ketone concentration is 300 mM. The NMR tube was immersed in liquid nitrogen, evacuated, and filled with H_2 at 1 atm, leading to an actual pressure of 4 atm at room temperature. The hydrogenation reaction proceeded at room temperature and was monitored by ^{1}H NMR spectroscopy. 3-Pentanone conversion was determined by ^{1}H NMR as the ratio between the amount of alcohol formed and the amount of catalyst present.

General Procedures for X-ray Crystallography. Pertinent details for the individual compounds can be found in Table 3.

Crystallographic data for compounds **3**, **4**, and **12** were collected using graphite-monochromated Mo Kα radiation (α = 0.710 73 Å) on a Bruker AXS-KAPPA APEX II area detector diffractometer equipped with an Oxford Cryosystem open-flow nitrogen cryostat, and data were collected at 150 K. Cell parameters were retrieved using Bruker SMART software and refined using Bruker SAINT on all observed reflections. Absorption corrections were applied using SADABS.[42] The structures were solved by direct methods using either SHELXS-97[43] or SIR 97[44] and refined using full-matrix least-squares refinement against F^2 using SHELXL-97.[43] All programs are included in the package of programs WINGX-version 1.64.05.[45] All non-hydrogen atoms were refined anisotropically, and all hydrogen atoms were placed in idealized positions and refined riding on the parent carbon atom. The molecular structures were drawn with ORTEP3 for Windows.[46] **3** and **4** data presented high values for residual electronic density located at special positions within the unit cell, which were ascribed to residual solvent molecules. Attempts to determine the position of the solvent disordered molecules led us to locate a diethyl ether molecule with the oxygen atom occupying a special position. The molecule has $^1/_4$ occupancy, and none of the disorder models attempted improved the refinement data. Complex **3** allowed an anisotropic refinement of the solvent molecule, while in complex **4** the solvent molecule was refined isotropically. During the refinement of the structure of compound **12** a significant solvent-accessible void was found, and as it was not possible to determine the solvent position, SQUEEZE[47] (PLATON[48]) was used. Data for complexes **3**, **4**, and **12** were deposited with the CCDC under the deposit numbers CCDC 684304, 684305, and 684306, respectively, and can be obtained free of charge from The Cambridge Crystallographic Data Centre via www.ccdc.cam.uk/data_request/cif.

Computational Details. All calculations reported in the text were performed using the Gaussian 03 software package[49] and the PBE1PBE functional, without symmetry constraints. That functional uses a hybrid generalized gradient approximation (GGA), including 25% mixture of Hartree−Fock[50] exchange with DFT[20] exchange correlation, given by the Perdew, Burke, and Ernzerhof functional (PBE).[51] The optimized geometries were obtained with the LanL2DZ basis set[52−55] augmented with an f-polarization function[56] for Mo and standard 6-31G(d,p) basis sets[57−61] for the remaining elements (basis b1). Transition state optimizations were performed with the synchronous transit-guided quasi-Newton method (STQN) developed by Schlegel et al.[62,63] Frequency calculations were performed to confirm the nature of the stationary points, yielding one imaginary frequency for the transition states and none for the minima. Each transition state was further confirmed by following its vibrational mode downhill on both sides and obtaining the minima presented on the energy profiles. A natural population analysis (NPA)[30−37] and the resulting Wiberg indices[28,29] were used to study the electronic structure and bonding of the optimized species.

The energy values presented in Figure 2 result from single-point energy calculations using a VTZP basis set (basis b2) and the

(42) SADABS: Area-Detector Absorption Correction; Siemens Industrial Automation, Inc., Madison, WI, 1996.
(43) Sheldrick, G. M. SHELXL-97: A Program for Refining Crystal Structures; University of Göttingen, Göttingen, Germany, 1998.
(44) Altomare, A.; Burla, M. C.; Camalli, M.; Cascarano, G.; Giacovazzo, C.; Guagliardi, A.; Moliterni, A. G. G.; Polidori, G.; Sparna, R. *J. Appl. Crystallogr.* **1999**, *32*, 115–119.
(45) Farrugia, L. J. *J. Appl. Crystallogr.* **1999**, *32*, 837–838.
(46) Farrugia, L. J. *J. Appl. Crystallogr.* **1997**, *30*, 565.
(47) Vandersluis, P.; Spek, A. L. *Acta Crystallogr., Sect. A* **1990**, *46*, 194–201.
(48) Spek, A. L. PLATON, A Multipurpose Crystallographic Tool; Utrecht University, Utrecht, The Netherlands, 1998.
(49) Frisch, M. J.; Trucks, G. W.; Schlegel, H. B.; Scuseria, G. E.; Robb, M. A.; Cheeseman, J. R.; Montgomery, J. A., Jr.; Vreven, T.; Kudin, K. N.; Burant, J. C.; Millam, J. M.; Iyengar, S. S.; Tomasi, J.; Barone, V.; Mennucci, B.; Cossi, M.; Scalmani, G.; Rega, N.; Petersson, G. A.; Nakatsuji, H.; Hada, M.; Ehara, M.; Toyota, K.; Fukuda, R.; Hasegawa, J.; Ishida, M.; Nakajima, T.; Honda, Y.; Kitao, O.; Nakai, H.; Klene, M.; Li, X.; Knox, J. E.; Hratchian, H. P.; Cross, J. B.; Adamo, C.; Jaramillo, J.; Gomperts, R.; Stratmann, R. E.; Yazyev, O.; Austin, A. J.; Cammi, R.; Pomelli, C.; Ochterski, J. W.; Ayala, P. Y.; Morokuma, K.; Voth, G. A.; Salvador, P.; Dannenberg, J. J.; Zakrzewski, V. G.; Dapprich, S.; Daniels, A. D.; Strain, M. C.; Farkas, O.; Malick, D. K.; Rabuck, A. D.; Raghavachari, K.; Foresman, J. B.; Ortiz, J. V.; Cui, Q.; Baboul, A. G.; Clifford, S.; Cioslowski, J.; Stefanov, B. B.; Liu, G.; Liashenko, A.; Piskorz, P.; Komaromi, I.; Martin, R. L.; Fox, D. J.; Keith, T.; Al-Laham, M. A.; Peng, C. Y.; Nanayakkara, A.; Challacombe, M.; Gill, P. M. W.; Johnson, B.; Chen, W.; Wong, M. W.; Gonzalez, C.; Pople, J. A. Gaussian 03, Revision C.02; Gaussian, Inc., Wallingford CT, 2004.
(50) Hehre, W. J.; Radom, L.; Schleyer, P. v. R.; Pople, J. A. *Ab Initio Molecular Orbital Theory*; Wiley: New York, 1986.
(51) Perdew, J. P.; Burke, K.; Ernzerhof, M. *Phys. Rev. Lett.* **1997**, *78*, 1396.
(52) Dunning, T. H., Jr.; Hay, P. J. *Modern Theoretical Chemistry*; Plenum: New York, 1976; p 1.
(53) Hay, P. J.; Wadt, W. R. *J. Chem. Phys.* **1985**, *82*, 270–283.
(54) Wadt, W. R.; Hay, P. J. *J. Chem. Phys.* **1985**, *82*, 284–298.
(55) Hay, P. J.; Wadt, W. R. *J. Chem. Phys.* **1985**, *82*, 299–310.
(56) Ehlers, A. W.; Bohme, M.; Dapprich, S.; Gobbi, A.; Hollwarth, A.; Jonas, V.; Kohler, K. F.; Stegmann, R.; Veldkamp, A.; Frenking, G. *Chem. Phys. Lett.* **1993**, *208*, 111–114.
(57) Ditchfie, R.; Hehre, W. J.; Pople, J. A. *J. Chem. Phys.* **1971**, *54*, 724–728.
(58) Hehre, W. J.; Ditchfie, R.; Pople, J. A. *J. Chem. Phys.* **1972**, *56*, 2257–2261.
(59) Harihara, P. C.; Pople, J. A. *Mol. Phys.* **1974**, *27*, 209–214.
(60) Gordon, M. S. *Chem. Phys. Lett.* **1980**, *76*, 163–168.
(61) Harihara, P. C.; Pople, J. A. *Theor. Chim. Acta* **1973**, *28*, 213–222.
(62) Haussermann, U.; Dolg, M.; Stoll, H.; Preuss, H.; Schwerdtfeger, P.; Pitzer, R. M. *Mol. Phys.* **1993**, *78*, 1211–1224.
(63) Kuchle, W.; Dolg, M.; Stoll, H.; Preuss, H. *J. Chem. Phys.* **1994**, *100*, 7535–7542.

geometries optimized at the PBE1PBE/b1 level. Basis b2 consisted of the Stuttgart/Dresden ECP with valence triple-ζ (SDD)[62−64] and an added f-polarization function[52] for Mo and standard 6-311++G-(d,p) basis sets[65−71] for the remaining elements. Solvent (dichloromethane) effects were considered in the PBE1PBE/b2//PBE1PBE/b1 energy calculations using the polarizable continuum model (PCM) initially devised by Tomasi and co-workers[72−74] as implemented on Gaussian 03,[75] and thus, the energy values in Figure 2 can be taken as free energy values.[76] The molecular cavity was based on the united atom topological model applied on UAHF radii, optimized for the HF/6-31G(d) level.

Acknowledgment. We thank the Fundação para a Ciência e a Tecnologia, Lisbon, Portugal, for funding (POCTI/QUI/55744/2004, SFRH/BD/13374/2003, SFRH/BPD/26745/2006).

Supporting Information Available: Tables giving atomic coordinates of all optimized species, CIF files giving X-ray crystallographic data for compounds **3**, **4**, and **12** and Figure S1, giving a free energy profile. This material is available free of charge via the Internet at http://pubs.acs.org.

OM800379Z

(64) Leininger, T.; Nicklass, A.; Stoll, H.; Dolg, M.; Schwerdtfeger, P. *J. Chem. Phys.* **1996**, *105*, 1052–1059.
(65) Mclean, A. D.; Chandler, G. S. *J. Chem. Phys.* **1980**, *72*, 5639–5648.
(66) Krishnan, R.; Binkley, J. S.; Seeger, R.; Pople, J. A. *J. Chem. Phys.* **1980**, *72*, 650–654.
(67) Wachters, A. J. *J. Chem. Phys.* **1970**, *52*, 1033–1036.
(68) Hay, P. J. *J. Chem. Phys.* **1977**, *66*, 4377–4384.
(69) Raghavachari, K.; Trucks, G. W. *J. Chem. Phys.* **1989**, *91*, 1062–1065.
(70) Curtiss, L. A.; Mcgrath, M. P.; Blaudeau, J. P.; Davis, N. E.; Binning, R. C.; Radom, L. *J. Chem. Phys.* **1995**, *103*, 6104–6113.
(71) Mcgrath, M. P.; Radom, L. *J. Chem. Phys.* **1991**, *94*, 511–516.
(72) Cances, E.; Mennucci, B.; Tomasi, J. *J. Chem. Phys.* **1997**, *107*, 3032–3041.
(73) Cossi, M.; Barone, V.; Mennucci, B.; Tomasi, J. *Chem. Phys. Lett.* **1998**, *286*, 253–260.
(74) Mennucci, B.; Tomasi, J. *J. Chem. Phys.* **1997**, *106*, 5151–5158.
(75) Tomasi, J.; Mennucci, B.; Cammi, R. *Chem. Rev.* **2005**, *105*, 2999–3093.
(76) Cossi, M.; Scalmani, G.; Rega, N.; Barone, V. *J. Chem. Phys.* **2002**, *117*, 43–54.